

Appendix B: I7

Here we discuss the details of the improvement in methods made as a result of utilizing experimental data (Bozza et al. 2002) and theory.

We predicted two sets of structures for M-I7 and R-I7. The first set of structures was predicted using the structure prediction algorithm MembStruk1.0 from Floriano et al. 2000. We refer to these structures as preMI7 and preRI7. The second set of structures used an improved MembStruk method (version 2.0) that includes the coarse grain optimization of the rotational orientation of the helices, called CoarseRot (described below). This step has improved the structures, as shown below, and we refer to the structures as M-I7 and R-I7. The reason that we report results for all these structures, is to show how the utilization between theory and experimental data have enabled the improvement of methods. Also, the docking results were originally carried out using the preM-I7 and preR-I7 structures. These results are a blind test, prior to having access to the experimental results from experiments (Bozza et al. 2002) and we felt that it was important to report both the answers we knew before we had access to the experimental results along with the answers we get with our new generation structures.

Details of the various methods used for predicting structure and function of rat and mouse I7 olfactory receptors (OR) are given below.

1.0 Force Fields

We used the Dreiding Force Field (FF) (Mayo et al. 1990) to describe the valence and van der Waals (vdW) interactions of the ligands and Gasteiger (Gasteiger et al. 1980) charges to describe the electrostatic (Coulomb) interactions. For the free ligand, the

dielectric constant was taken as 1.0, and there were no cutoffs in the VdW and Coulomb interactions.

For the protein we used the Dreiding FF with CHARMM charges. Here we used a dielectric constant of 1.0 and the Cell Multipole Method (CMM, Ding *et al.* 1992a,b) for calculating the vdW and coulomb interactions. The solvation energies and forces for the odorants were calculated using the Analytical Volume Generalized Born (AVGB) continuum solvation method using a dielectric constant of 78.2 for outside the protein and 1.3 for inside the protein.

2.0 MembStruk Procedure for Predicting Structure of M-I7 and R-I7

The details of MembStruk1.0 and MembStruk2.0 are described elsewhere (Floriano *et al.*, 2000; Vaidehi *et al.*, 2002), but we will summarize the various steps in a MembStruk1.0 prediction (improvements to version 2.0 described in Section 5.0) using M-I7 as the example.

2.1 TMPred: Predict helical regions from hydrophobicity profiles:

The TM helices were identified for ORs on the basis of hydrophobicity by the multisequence profile method, of Donnelly 1993, implemented in PERSCAN. To do this, we aligned the sequences for M-I7 and R-I7 along with 21 other rat and mouse OR's that had similar homology, and used these alignments in PERSCAN to predict the TM region based on hydrophobicity profiles. (See Figure 1). These predicted TM regions were used to build canonical right-handed α -helices.

We then oriented each helical axis to match the 7.5Å electron density map from frog rhodopsin (Schertler 1998). The barrel of seven TM helices of the GPCR is surrounded by the lipid bilayer (membrane). The residues bordering the membrane

are expected to be hydrophobic, while hydrophilic residues are expected to point toward the internal regions or toward other helices. Thus we take the initial position of each TM region to have its net hydrophobic moment point outward from the center of the barrel of seven helices.

2.2 Optimization of the TM region

The structures of these helices were optimized using NEIMO (Newton-Euler Inverse Mass Operator) torsion MD (Jain et al. 1993, Mathiowetz et al. 1994, Vaidehi et al. 1996), which allows all torsion angles to change, but keeps the bonds and angles fixed.

2.3 Optimization of the helical bundle

Starting with the optimized seven-helix barrel, we packed 100 lipid molecules (DPC) around the helices and optimized the lipid region (as rigid bodies) while keeping the TM barrel rigid. This rigid body dynamics was carried out for 100 ps in MpSim (Lim *et al.*, 1997) to ensure equilibration.

2.4 Full atomic Optimization:

Following the rigid body dynamics, loops were added to the helices using the WHATIF (Vriend 1990) software. After the addition of loops we performed a full atom minimization of the loops (leaving the TMR fixed) until a RMS of 0.5 has been achieved, then full minimization of the complete GPCR.

3.0 Preparation of the odorant library for docking studies:

We were provided with the names of the 56 molecules that had been tested for activity on M-I7 and R-I7 ORs (Bozza private communication), but were not provided any information about the binding site or the measured odorant binding profile. This set

of 56 molecules includes alcohols, carboxylic acids, esters, ethers, aldehydes, and ketones. Including stereoisomers leads to the 62 ligands shown in Table I of the publication. For each molecule, we constructed the extended conformation and minimized the structure using conjugate gradients. These minimized conformations were used as starting conformations for HierDock. The acids and possibly charged odorants were considered in both charged and neutral forms for docking. The analysis of the docking site used whichever charge gave the best docking energy.

The receptor/odorant complexes were then ranked according to the predicted binding affinities. These results are in Table IV of the publication.

4.0 The HierDock2.0 Procedure for Predicting Binding Site and Binding Energy

We used the HierDock2.0 procedure (Floriano et al., 2000) to predict the odorant binding sites and binding energies in M-I7 and R-I7 ORs. HierDock is a hierarchical docking strategy consisting of a coarse grain docking method to generate ligand/protein bound structures followed by fine grain all atom optimization of a certain number of these complexes using continuum solvation methods. HierDock has been validated for other ORs (Floriano et al. 2000), other GPCRs (Vaidehi et al. 2002), and also globular proteins (Wang et al. 2002; Datta et al. 2002). The details of the HierDock2.0 protocol are described elsewhere (Floriano et al. 2000, Vaidehi et al. 2002, Wang et al. 2002), but we summarize the main elements of the procedure as applied to odorant docking to the ORs.

4.1 Scanning the entire receptor for potential binding sites

For each of the 62 ligands in Table 1 of the publication, we scanned for possible binding regions across the entire receptor (except for the intracellular

loops and the part in contact with the membrane). These regions used for docking were described using spheres generated over the whole receptor (using the Sphgen program in DOCK4.0), partitioned into 13 overlapping cubic docking boxes each with a side of 10Å, as shown in Appendix Figure 2. We then performed HierDock calculations in each of these 13 regions. The steps are as follows:

a. Coarse Docking: Using Dock 4.0 (Ewing 1997) we generated 1000 conformations for each of the 62 odorants in the two receptors preM-I7 and preR-I7. We used the flexible ligand docking option with torsion minimization, a non-distance dependent dielectric constant of 1, and a cutoff of 10 Å for energy evaluation. The conformations were ranked using energy scoring function from DOCK4.0. The best scoring 10% (100 conformations) for *each* odorant in *each* of the 13 binding regions were used as input for the next step of finer refinement of conformations and energy evaluation.

b. Ligand optimization: The next step is to select a subset of the docked ligands using a better FF and optimizing the structure of the ligand with protein fixed. Here we used the Dreiding FF and Gasteiger charges for the ligands and calculated energy of the ligand with protein fixed using the all-atom Dreiding forcefield. We did for each of the 100 structures from level a. For each of these 100 minimized structures we calculated the amount of the ligand surface that is buried in the receptor using Connolly's MS program from QCPE (Connolly, 1983). For each box and each ligand we then selected the best energy structure with a buried surface area above 90%.

c. *Selection of the binding region:* The above steps a and b were performed for each of the 62 ligands in table I of the publication for each of the 13 potential binding regions. For each ligand we determined the protein binding site by selecting the region with the best binding energy. We then considered the final coordinates of all the ligands in their binding site and then defined the "binding site" as the average of the center of mass of the ligands in a 3Å radius cluster that contained the highest number of ligands. We then defined the putative binding region as a cube with 10Å on each side centered at this site. This binding region was determined independently for R-I7 and M-I7.

4.2. Determining the binding conformation and binding energies for all the ligands

The entire library of 62 odorants was docked into the putative binding region, repeating steps a and b of HierDock for just this region. This leads to 100 conformations for each ligand. Of these we selected (for each of the 62 odorants) the 10% (10 conformations) with the lowest energies for the next step.

4.3. Optimizing bound ligand-receptor complex for all the ligands

To determine the best binding conformation of each ligand in the receptor, it is important to allow both the ligand *and the receptor* to optimize their conformations. Thus the 10 best scoring structures from step d were minimized allowing all atoms of both protein and ligand to be optimized. Each structure was scored using the binding energies:

$$BE = PE (\text{odorant in water}) - PE (\text{odorant in the receptor}). \quad (1)$$

where BE is the binding energy of the odorant in the receptor, PE (odorant in receptor) is the potential energy of the odorant calculated with the OR fixed. PE (odorant in water) is the potential energy of the odorant in water calculated for the starting conformation of the ligand. Even though the protein was allowed to relax in step 4, the potential energy of the odorant in the receptor in (1) was calculated using DREIDING force field with the receptor atoms fixed. The PE of the odorant in water was calculated using the AVGB continuum solvation method.

4.4 Binding energies calculated for odorants in the preM-I7 and preR-I7 structures

The preM-I7 and preR-I7 structures were used for the odorant binding profile predictions showed in Table IV of the publication. About 10 aldehydes were predicted to be good binders to both R-I7 and M-I7, suggesting that this receptor is an aldehyde receptor. However our predictions showed that heptanal and octanal both bind equally well to both preR-I7 and preM-I7 receptors. This is contrary to the results in current literature (Krautwurst et al. 1998) that reported only heptanal binds to R-I7 while only octanal binds to M-I7.

As indicated in Table IV of the publication, the predicted binding is in fair agreement with experiment. In particular the experimental data also showed that both heptanal and octanal bind to both M-I7 and R-I7 as we had predicted. Although there were several false positives (e.g. linal, lylal, decanal), Table IV indicates that the blind predictions correctly predicted that aldehydes would activate R-I7 and M-I7.

4.5 Binding site analysis for the preM-I7 and preR-I7 structures

Along with the binding energies a look at the specific residues and their positions in the binding site were analyzed. The final position of heptanal in preM-I7 and the final position of octanal in preR-I7 from the HierDock2.0 protocol were used to look at the hydrogen bonding and relative distances of the residues. These results are found in Appendix Figure 3. The distances show that these structures are relatively loose fitting in the binding site and are not always hydrogen bonded to Lys164. However, the binding site is still in agreement with other results that present that binding happens in the TM3 – TM7 region as seen with D2 (Kalani et. al. PNAS 2004 – reference in main document). This gives the descent binding energies that compare to experiments.

5.0 Refinement of Computational Methods and Results

In the original formulation of MembStruk, described above in section 2.0, the first step 2.1 above was followed by steps 2.2 to 2.2.4. However in applying this method to various systems we found the MembStruk1.0 was not optimized to give the best energy orientation of the helices. Without coarse grain optimizations, fine grain molecular dynamics (MD) like the rigid body MD does not provide adequate sampling of orientations of the helices. In studying these systems, we concluded that it was necessary to scan through large ranges of these orientations to go over barriers to sample new orientations that may have better energies. We also learned that that it was important to allow the neighboring helices reorient and to allow the side chains to reoptimize for the changes in rotational orientation of the helices. Hence, we developed the improvement to MembStruk to include a step to scan over a large region of orientations called *CoarseRot*

shown below. This new step would come right after step 2.2, and followed by the steps 2.3 to 2.5.

5.1 CoarseRot: Hydrophobic analysis and mesoscale rotation method

Since the orientation of the helical axes and their tilts with respect to each other are critical factors in determining the conformation of the ligand-binding site in GPCRs, we developed the coarse grain CoarseRot procedure to optimize the rotations and translation of each helix in the seven helical TM barrel. There are two methods involved in CoarseRot:

- 1) CoarseRot-E optimizes with respect to the total energy (most important for TM3)
- 2) CoarseRot-H orients the net hydrophobic moment of each helix pointing to be toward the membrane (most important for the other six TMs).

In the CoarseRot-E procedure, each of the seven TM's is optimize through a range of rotations and translation one at a time (the active TM) while the other helices are reoptimized in response. The active TM is allowed to rotate through the range of rotation angles about its helical axis in which its net hydrophobic moment points outwards. After each rotation of the main chain (kept rigid) the side chain positions of all residues for all seven helices in the TMR are optimized using SCWRL (Bower et. al. 1997). The atoms of the active helix is then fully conjugate gradient minimized till an RMS of 0.5 is achieved or 80 steps of minimization have occurred in the field of all the other helices (all atoms fixed) using with the DREIDING all-atom force field (Mayo et al., 1990). This procedure is carried out for a grid of rotation angles for the active helix to

determine the optimum rotation for the active helix. Keeping the active helix in its optimum rotated conformation, we then allow each of the other six helices to be rotated and optimized. Here we rotate the main chain, SCWRL the side chains and then optimize the atoms of each of the six helices one by one. The optimization of these six helices is done iteratively until there is no further lowering of energy. This method is most important for TM 3, which is near the center of the protein and not particularly amphipathic (it has a small hydrophobic moment due to several charged residues) (see Appendix Figure 1).

In the CoarseRot-H procedure, the hydrophobic moment is calculated for the middle portion of each helix (typically the middle 1/3 or ~ 15). The hydrophobicity vector is then projected onto the common helical plane to point farthest away from the two nearest TMs or else it is oriented exactly opposite to the direction toward the geometric center of the TM barrel. The helical plane is defined as the plane that most closely intersects the geometrical midpoints of all seven TM helices. The midpoint is calculated from the positions of the alpha carbon from each residue in the helix. After positioning the hydrophobic vectors, we search over a grid of small rotations ($\sim 10^\circ$) and translations ($\sim 1\text{\AA}$) for each helix to find a position for each of the seven helices that maximizes the number of salt bridges and hydrogen bonds *between* helices. This method is most appropriate for the six helices having significant contacts with the lipid membrane, since the hydrophobic moments pointing towards the membrane.

The full CoarseRot protocol combines both the energy optimization and hydrophobic moments should provide even better adjustments to the geometry of

the structures and better correlation of the predicted binding profiles to experimental data. To distinguish the results using CoarseRot from those that did not, we refer to the latter structures (predicted with MembStruk in section 2.0) as preM-I7 and preR-I7.

6.0 Results For The Refined Computational Methods

Simultaneously with carrying out the binding studies in Table IV of the publication, we had been developing the CoarseRot method to better optimize the TM regions for GPCRs and had tested it for bovine rhodopsin and some other GPCRs (Vaidehi et al 2002, Trabanino et al 2003).

6.1 Improving the M-I7 and R-I7 Predicted Structures

Consequently after receiving the experimental results, we proceeded to predicted odorant binding profiles for the new structures of the receptors. The new M-I7 structure was found to lead to excellent correlation with the experimental results. This M-I7 structure differed from the original preM-I7 structure by rotating TM1 by 15°, TM3 by 15°, TM4 by 5°, and TM5 by -80°. The rotation angles chosen were automatically determined by the CoarseRot algorithm detailed in section 5.1. Thus a generic improvement in the MembStruk method eliminated the few false positives in the original predictions.

This improved the agreement between the calculated binding energies and experimental odorant activation profile for M-I7 structure. On the other hand the agreement of the predictions for R-I7 was less impressive. Since the sequences of M-I7 and R-I7 differ by only 15 mutations, we decided to generate the homology based structure for R-I7 by mutating the predicted structure for M-I7 and then

reoptimizing this predicted structure. This structure is denoted as R-I7(hom) (homology structure of rat I7 obtained from mouse structure, M-I7 as template). The results of docking the odorant library to M-I7 and R-I7(hom) are shown in Table V of the publication, where we see a good correlation with experimental results.

7.0 REFERENCES

- Araneda, R. C., Kini, A. D., and Firestein, S. (2000). The molecular receptive range of an odorant receptor. *Nat. Neuroscience* 3(12), 1248-1255.
- Araneda, S., Mermet, N., Verjat, T., Angulo, J. F., and Radicella, J. P. (2001). Expression of Kin17 and 8-OxoG DNA glycosylase in cells of rodent and quail central nervous system. *Brain Res. Bull.* 56(2), 139-46.
- Bower, M., Cohen, F. E., and Dunbrack, R. L., Jr. (1997). Prediction of protein side-chain rotamers from a backbone-dependent rotamer library: a new homology modeling tool. *J. Mol. Biol.* 267, 1268-1282
- Bozza, T., and Kauer, J. S. (1998). *Odorant response properties of convergent olfactory receptor neurons.* *J. Neurosci.* 18, 4560-4569.
- Bozza, T., Feinstein, P., Zheng, C., and Mombaerts, P. (2002). Odorant Receptor Expression Defines Functional Units in the Mouse Olfactory System. *J. of Neuroscience* 22(8), 3033-3043
- Buck, L., Axel, R., (1991). A Novel Multigene Family May Encode Odorant Receptors: A Molecular Basis for Odor Recognition. *Cell* 65, 175-187.
- Connolly, M. L. (1983). Solvent-Accessible Surfaces of Proteins and Nucleic Acids. *Science* 221(4612), 709-713.
- Cromarty, S. I., Derby, C. D. (1998). Inhibitory receptor binding events among the components of complex mixtures contribute to mixture suppression in responses of olfactory receptor neurons of spiny lobsters. *J. Comparative Physiology A - Sensory Neural And Behavioral Physiology.* 183, 699-707.
- Ding, H. Q., Karasawa, N., and Goddard III, W.A. (1992). Atomic level simulations on a million particles: The cell multipole method for Coulomb and London nonbond interactions. *J. Chem. Phys.* 97(6), 4309-4315.
- Ding, H. Q., Karasawa, N., and Goddard III, W. A. (1992). Atomic level simulations on a million particles: The cell multipole method for Coulomb and London nonbond interactions. *Chem. Phys. Lett.* 196(1), 6-10.
- Donnelly, D. (1993). Modelling alpha-helical transmembrane domains. *Biochem. Soc. T.* 21(1), 36-39.
- Duchamp-Viret, P., Chaput, M. A., and Duchamp, A. (1999). Odor Response Properties of Rat Olfactory Receptor Neurons. *Science.* 284, 2171-2174
- Eisenberg D., Weiss R. M., Terwilliger, T. C., (1984). The Hydrophobic Moment Detects Periodicity In Protein Hydrophobicity. *Proc. Natl. Acad. Sci. USA,* 8, 140-144.
- Ewing, T. A. and Kuntz, I. D. (1997). Critical evaluation of search algorithms for automated molecular docking and database screening. *J Comput. Chem.* 18(9), 1175-1189.

- Floriano, W. B., Vaidehi, N., Singer, M. S., Shepherd, G. M., Goddard III, W. A. (2000). Molecular Mechanisms underlying differential odor responses of a mouse olfactory receptor. *P. Natl. Acad. Sci. USA* 97, 10712-10716.
- Freddolino, P. L., Kalani, M. Y., Vaidehi, N., Floriano, W. B., Hall, S. E., Trabanino, R. J., Kam, V., and Goddard III W. A. (2004). 3D Structure for Human β 2 Adrenergic Receptor and the binding site for Agonists and Antagonist. *PNAS* 101, 2736-2741
- Gasteiger J, Marsili M. (1980). Iterative partial equalization of orbital electronegativity—a rapid access to atomic charges. *Tetrahedron* 36(22), 3219-3228.
- Ghosh, A., Rapp, C. S., and Friesner, R. A. (1998). Generalized Born Model Based on a Surface Integral Formulation. *J. Phys. Chem. B* 102(52), 10983-10990.
- Gimenez C. (1998). Composition and structure of the neuronal membrane: molecular basis of its physiology and pathology. *Rev Neurol* 26(15), 232-239.
- Godfrey P. A., Malnic, B., and Buck, L. B., (2004). The mouse olfactory receptor gene family, *Proc. Natl. Acad. Sci. USA*, 101, 2156-2161.
- Grigorieff, N., Ceska, T. A., Downing, K. H., Baldwin, J. M., and Henderson, R. (1996). Electron-crystallographic Refinement of the Structure of Bacteriorhodopsin. *J. Mol. Biol.* 259(3), 393-421.
- JAGUAR v. 4.0— Schrodinger Co, Portland Oregon.
- Jain, A., Vaidehi, N. and Rodriguez, G. (1993). A Fast Recursive Algorithm for Molecular Dynamics Simulation. *J. Comp. Phys.* 106(2), 258-268.
- Kajiya, K., Inaki, K., Tanaka, M., Haga, T., Kataoka, H., and Touhara, K. (2001). Molecular bases of odor discrimination: Reconstitution of olfactory receptors that recognize overlapping sets of odorants. *J. of Neuroscience* 21(16), 6018-6025 Aug. 15
- Kalani, M. Y., Vaidehi, N., Freddolino P. E., Floriano W. B., Hall, S. E., Trabanino, R. J., Kam V., and Goddard III, W. A. (2004). Structure and function of human D_{2L} receptor, *PNAS* 101, 3815-3820
- Kiefer, H., Krieger, J., Olszewski, J. D., von Heijne, G., Prestwich G. D., Breer H. (1996). Expression of an Olfactory Receptor in *Escherichia coli*: Purification, Reconstitution, and Ligand Binding. *Biochemistry* 35(50), 16077-16084.
- Krautwurst, D., Yau, K. W. and Reed, R. R. (1998). Identification of Ligands for Olfactory Receptors by Functional Expression of a Receptor Library. *Cell* 95(7), 917-926.
- Kuntz I. D., Blaney J. M., Oatley S. J., Langridge R., Ferrin T. E. (1982). A geometric approach to macromolecule-ligand interactions. *J. Mol. Biol.* 161(2), 269-288.
- Lancet, D., Sadovsky, E., Seidemann, E. (1993). Probability model for molecular recognition in biological receptor repertoires: significance to the olfactory system. *Proc Natl Acad Sci U S A.* 90(8), 3715-9.

- Levasseur, G., Persuy, M., Grebert, D., Remy, J., Salesse, R., and Pajot-Augy, E. (2003). Ligand-specific dose-response of heterologously expressed olfactory receptors. *Eur. J. Biochem.* 270(13), 2905-2912
- Lim, K-T, Brunett, S., Iotov, M., McClurg, R. B., Vaidehi, N., Dasgupta, S., Taylor, S. and Goddard III, W. A. (1997). Molecular dynamics for very large systems on massively parallel computers: The MPSim program. *J Comput. Chem.* 18(4), 501-521.
- MacKerell, A. D., Bashford, D., Bellott, M., Dunbrack, R.L., Evanseck, J.D., Field, M. J., Fischer, S., Gao, J., Guo, H., Ha, S., Joseph-McCarthy, D., Kuchnir, L., Kuczera, K., Lau, F. T. K., Mattos, C., Michnick, S., Ngo, T., Nguyen, D. T., Prodhom, B., Reiher, W. E., Roux, B., Schlenkrich, M., Smith, J.C., Stote, R., Straub, J., Watanabe, M., Wiorkiewicz-Kuczera, J., Yin, D. and Karplus, M. (1998). All-Atom Empirical Potential for Molecular Modeling and Dynamics Studies of Proteins. *J. Phys. Chem. B* 102(18), 3586-3616.
- Malnic, B., Hirono, J., Sato, T., and Buck, L. B. (1999). Combinatorial Receptor Codes for Odors. *Cell* 96(5), 713-723.
- Malnic B., Godfrey P. A., and Buck, L. B., (2004). The human olfactory receptor gene family, *Proc. Natl. Acad. Sci. USA*, 101, 2584-2589.
- Filizola, M., Perez, J. J., and Carteni-Farine, M. (1998). BUNDLE: A program for building the transmembrane domains of G-protein-coupled receptors. *J. Computer-Aided Molecular Design* 12, 111-118
- Mathiowetz, A. M., Jain, A., Karasawa, N., and Goddard III, W. A. (1994). Protein Simulations using Techniques Suitable for Very Large Systems: the Cell Multipole Method for Nonbond Interactions and the Newton-Euler Inverse Mass Operator Method for Internal Coordinate Dynamics. *Proteins* 20, 227.
- Mayo, S. L., Olafson, B. D. and Goddard III, W. A. (1990). DREIDING: a generic force field for molecular simulations. *J. Phys. Chem.* 94(26), 8897-8909.
- Mombaerts P. (1999). Seven-transmembrane proteins as odorant and chemosensory receptors. *Science* 286(5440), 707-711.
- Mori, K., Nagao, H., and Yoshihara, Y. (1999). The Olfactory Bulb: Coding and Processing of Odor Molecule Information. *Science* 286, 711-715.
- Palczewski, K., Kumasaka, T., Hori, T., Behnke, C., Motoshima, H., Fox, B., Trong, I., Teller, D., Okada, T., Stenkamp, R., Yamamoto, M., and Miyano, M. (2000). Crystal structure of rhodopsin: a G-protein-coupled receptor. *Science.* 289,739-745.
- Pilpel, Y., Lancet, D. (1999). The variable and conserved interfaces of modeled olfactory receptor proteins. *Prot. Sci.* 8(5), 969-977.
- Poincelot, R. P., Millar, P. G., Kimbel, R. L, Jr., Abrahamson, E. W. (1970). Determination of the chromophoric binding site in native bovine rhodopsin. *Biochemistry* 9(8), 1809-1816.
- Rappé, A.K. and Goddard III, W. A. (1991). Charge equilibration for molecular dynamics simulations. *J. Phys. Chem.* 95(8), 3358.

- Rubin, B. D., and Katz, L. C. (1999). Optical Imaging of Odorant Representations in the Mammalian Olfactory Bulb. *Neuron*. 23, 499-511.
- Sachdeva, A., Sachdeva O. P., Gulati S. P., Kakkar V. (1993). Nasal mucociliary clearance & mucus pH in patients with diabetes mellitus. *Indian J. Med. Res. B* 98, 265-268.
- Schertler, G.F.X. (1998). Structure of rhodopsin. *Eye* 12, 504-510.
- Sicard, G., and Holley, A. (1984). Receptor cell responses to odorants – similarities and differences among odorants. *Brain Res.* 292, 283-296
- Singer, M. S. (2000). Analysis of the Molecular Basis for Octanal Interactions in the Expressed Rat I7 Olfactory Receptor. *Chem. Senses* 25, 155-165
- Singer, M. S. and Shepherd, G. M. (1994). Molecular modeling of ligand-receptor interactions in the OR5 olfactory receptor. *Neuroreport. NeuroReport* 5(10), 1297-300.
- Singer, M.S., Weisinger-Lewin, Y., Lancet, D. and Shepherd, G.M. (1995a). Positive selection moments identify potential functional residues in human olfactory receptors. *Receptors Channels* 4(3), 141-147.
- Singer, MS, Oliveira L., Vriend G., and Shepherd G. M. (1995b). Potential ligand-binding residues in rat olfactory receptors identified by correlated mutation analysis. *Receptors Channels*, 3(2), 89-95
- Strader, C. D., Sigal, I. S. and Dixon R.A.F. (1989). Structural basis of beta-adrenergic receptor function. *FASEB J.* 3(7), 1825-1832.
- Tannor, D. J., Marten, B., Murphy, R., Friesner, R. A., Sitkoff, D., Nicholls, A., Ringnalda, M., Goddard III, W. A. and Honig, B. (1994). Accurate First Principles Calculation of Molecular Charge Distributions and Solvation Energies from Ab Initio Quantum Mechanics and Continuum Dielectric Theory. *J. Am. Chem. Soc.* 116(26), 11875.
- Trabanino R. J., Hall, S. E., Vaidehi N., Floriano W. B., and Goddard III, W. A. (2004). First Principles Predictions of the Structure and Function of G-Protein Coupled Receptors: Validation for Bovine Rhodopsin. *BioPhys. J.* 86, 1904-1921
- Vaidehi, N., Jain, A., & Goddard III, W.A. (1996). Constant Temperature Constrained Molecular Dynamics: The Newton-Euler Inverse Mass Operator Method. *J. Phys. Chem.* 100(25), 10508.
- Vaidehi, N., Floriano, W. B., Trabanino, R., Hall, S. E., Freddolino, P., Choi, E. J., Zamanakos, G., and Goddard III, W. A., (2002). Prediction of structure and function of G protein-coupled receptors. *Proc. Nat. Acad. Sci.* 99(20), 12622-12627.
- Vriend, G. (1990). WHAT IF: A molecular modeling and drug design program. *J. Mol. Graph.* 8(1), 52-56.
- Wetzel, C. H., Oles, M., Wellerdieck, C., Kuczkowiak, M., Gisselmann, G., Hatt, H. (1999). Specificity and sensitivity of a human olfactory receptor functionally expressed

in human embryonic kidney 293 cells and *Xenopus Laevis* oocytes. *J Neurosci* 19, 7426-7433.

Zamanakos, G. (2001). A fast and accurate analytical method for the computation of solvent effects in molecular simulations. *PhD Thesis, Physics, California Institute of Technology, Pasadena, CA*

Zhao, H., Ivic, L., Otaki, J. M., Hashimoto, M., Mikoshiba, K., Firestein, S., (1998). Functional Expression of a Mammalian Odorant Receptor. *Science*. 279, 237-241

I7 Appendix Figures

Figure 1 - Perscan Hydrophobic Moments

Shown in this figure are the relative positions of the TM regions 1 through 7 and their respective hydrophobic moments pointing in the positions originally dictated by PERSCAN (Donnelly 1993).

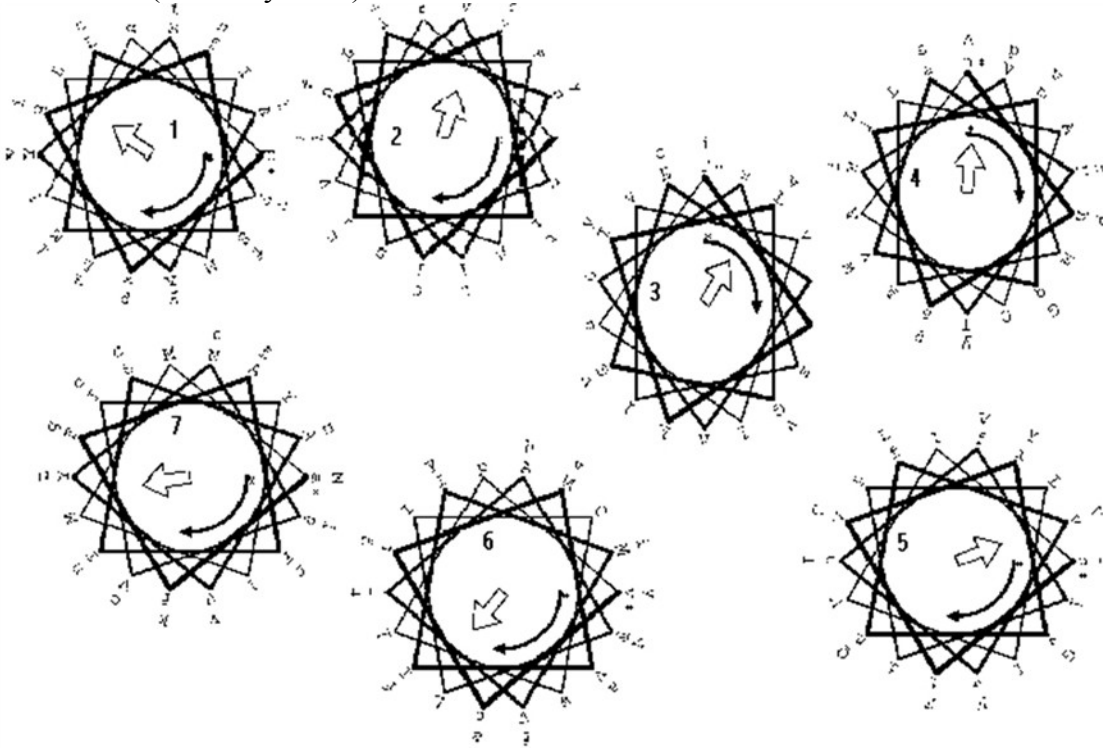


Figure 2 - preI7 Rat with Docking Boxes

This figure shows the position of the 13 binding boxes on the preRI7 model for scanning the model for a binding site.

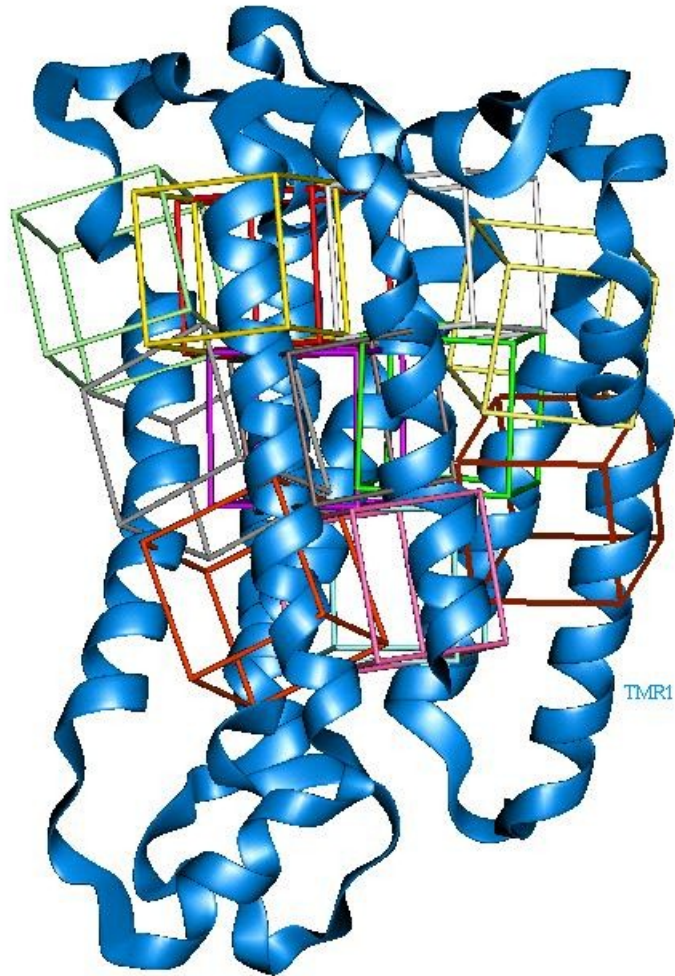
preI7 Rat with Docking Boxes

Figure 3 - Binding site distances for I7 Mouse and Rat

The figure shows the distances from the heavy atoms in the side chains of each residue to the non-hydrogen atoms of the respective antagonists for preM-I7 (heptanal) and preR-I7 (octanal). Where hydrogen bonding is present a “HB” will be next to the distance.

Mouse I7		
Residue	TM Region	Min Dist. from Ligand
Phe 109	TM3	3.9
Gly 113	TM3	3.8
Cys 114	TM3	3.2
Cys 117	TM3	3.6
Lys 154	TM4	3.4 HB
Tyr 173	LP4	2.9
Leu 212	TM5	4.6
Ile 255	TM6	4.4
Ala 259	TM6	4.6
Ser 280	TM7	5.2
Val 281	TM7	3.7
Ala 284	TM7	3.8

Rat I7		
Residue	TM Region	Min Dist. from Ligand
Phe 109	TM3	3.8
Leu 110	TM3	4.5
Gly 113	TM3	4.7
Cys 114	TM3	3.6 HB
Lys 154	TM4	3.1
Ile 255	TM6	4.6
Ala 259	TM6	4.1
Ala 260	TM6	4.1
Ser 280	TM7	4.7